Dynamics of Electron Injection and Recombination of Dye-Sensitized TiO_2 Particles

Marcus Hilgendorff and Villy Sundström*

Department of Chemical Physics, Lund University, P.O. Box 124, S-22100 Lund, Sweden

Received: May 12, 1998; In Final Form: September 11, 1998

Electron injection and recombination dynamics of the dye fluorescein 27 adsorbed on a titanium dioxide (TiO_2, anatase) surface were studied, following femtosecond pulse excitation of the 0−0 transition of the dye molecule. Nanosized colloidal particles (average diameter ∼ 2.4 nm) were employed as electron acceptors in optically transparent aqueous suspensions. Large changes of the dye absorption spectrum in the presence of TiO_2 colloids confirmed strong adsorption of the dye to the TiO_2 surface. The strong quenching of steady-state fluorescence under such conditions is correlated to the electron injection process. Transient absorption spectra and kinetics were recorded in the spectral region from 410 to 950 nm. While the transient absorption signal in the interval 410−600 nm originates primarily from the dye molecule, the observed signal in the range 600−950 nm is assigned to intra-band transitions or free carrier absorption of the electron injected into the semiconductor. The decay time of the stimulated emission of the dye and the rise time of the absorption of the injected electron reveal that electron injection into the TiO_2 colloid occurs with a characteristic time constant of 300 fs. In contrast, the analysis of the overall signal decay resulted in multiphasic recombination times, ranging from ∼10 picoseconds up to nano- or even microseconds. A red shift of the absorption maximum of the semioxidized radical anion (the product of electron injection) within ∼25 ps suggests vibrational cooling, solvation, or structural relaxation of the initially hot product. This provides strong evidence for a dynamic process involving relaxation of the potential energy of the radical on this time scale, leading to a dramatic decrease of the recombination reaction rate with time.

I. Introduction

Sensitization of semiconductors has been studied extensively in the past.[5,30] One of the earliest applications was in the photographic process,[1] involving the sensitization of silver halogens; electrophotography is another widespread application. The sensitization of wide band gap semiconductors (such as, for instance, ZnO, SnO_2, and TiO_2) has been suggested as an efficient tool in the conversion of light to electricity.[2−5,43] This process involves the excitation of dye molecules with visible light (eq 1) and the subsequent electron injection into a semiconductor, here assumed to be TiO_2 (eq 2):

$$\text{dye} \xrightarrow{h\nu} \text{dye}^* \tag{1}$$

$$\text{dye}^* \xrightarrow{TiO_2} \text{dye}^+ + e^- \tag{2}$$

High efficiencies for converting absorbed light into electricity rely on a fast electron injection combined with a very slow back reaction (eq 3):[6]

$$\text{dye}^+ + e^- \rightarrow \text{dye}$$

Recombination rates for different dyes were reported to range from several nanoseconds up to microseconds[7,8,10,11,40] and even milliseconds.[9] In comparison, the rate of electron injection has recently been reported to be in the femtosecond time domain.[11,12,36] Thus, high yields of a long-lived charge separation can be expected, implying that an application for the conversion of sunlight into electric charge (as achieved by natural photosynthetic membranes) appears to be feasible. Indeed, a very promising type of photo electrochemical solar cell has recently been developed by Grätzel and co-workers.[6] This device employs a nanocrystalline TiO_2 film covered with a monolayer of an adsorbed sensitizing dye, which is attached to a conducting glass plate. High conversion efficiencies for solar light were reported with certain ruthenium(II)-trisbipiridyl complexes used as sensitizers; in particular, conversion efficiencies of up to 10% were achieved with the Ru^{II}(2,2′-bipyridyl-4,4′-dicarboxylate)$_2$-$(NCS)_2$-dye.[6,9,11] In these solar cells the adsorbed dye is optically excited and subsequently injects an electron into a polycrystalline semiconductor layer, through which the electron migrates to an electrical back contact. The dye becomes oxidized and must therefore be regenerated by a redox system in contact with the adsorbed dye to sustain a cyclic process. The redox system itself is in contact with a counter electrode, usually a thin, transparent platinum film on a glass plate which rereduces the electrolyte. The electrical circuit is closed by contacting the counter electrode with the TiO_2 electrode via a load. For an efficient process it is necessary to establish conditions of both fast electron injection (to prevent degrading side reactions) and slow recombination (to allow time for a complete rereduction of the oxidized dye through the redox system). However, the detailed mechanisms, the nature and the rate of the electron injection into the semiconductor, and the factors determining the speed of the back reaction are not well understood.[10,11] Such information is of course important in the design of more efficient photo electrochemical solar cells. Furthermore, a better understanding of charge-transfer reactions at semiconductor surfaces could lead to improvements in all processes employing sensitization effects (i.e., photography, electro photography, surface catalytic mechanisms, and imaging).

* Author to whom correspondence should be addressed.

10.1021/jp982210s CCC: $15.00
Published on Web 11/26/1998

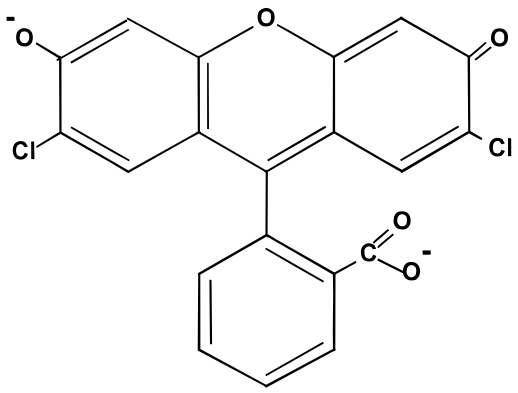

Figure 1. The sensitizing dye, fluorescein 27. Dianionic form.

We have studied in detail the ultrafast kinetics of charge injection and recombination in the sensitization of nanocrystalline TiO_2 semiconductor particles by the xanthene dye fluorescein 27 (see Figure 1). The nanocrystalline anatase particles have an average diameter of 2.4 nm.[14] The very small particle size and correspondingly large specific surface area, combined with the absence of light scattering in the visible spectral region, makes it possible to study light-induced reactions at the colloid surface with a good signal-to-noise ratio. Furthermore, the application of nanosized TiO_2 colloids enables establishment of conditions in which one electron is injected into one particle, thus mimicking the conditions of low light intensities prevailing in natural sunlight. The fluorescein 27 dye was found to be a suitable model compound for studies of charge injection, since these processes are already well characterized for several xanthene dyes, although no study of the ultrafast processes has been reported yet. In addition, the singlet excited state of fluorescein 27 has a nanosecond lifetime combined with a very low probability of triplet state formation and is therefore used as laser dye. In general, xanthene dyes exhibit intense ground-state absorption (maximum around 500 nm), which could make them, in principle, suitable sunlight harvesting agents.[8]

The charge injection of the xanthene dyes fluorescein, eosin Y, erythrosine B, and rose bengale adsorbed at ZnO or TiO_2 electrodes or particles, is a well-known process.[2,5,13] Moreover, the charge injection from eosin into colloidal TiO_2 particles has been studied with nanosecond and picosecond time resolution.[8,13] Moser et al.[8,13] assumed a rate constant for the electron transfer of $9.5 \times 10^8\ s^{-1}$ from their measurements and a quantum yield for charge separation of 38%. However, as mentioned above, more recent investigations with other sensitizing molecules show that the charge transfer occurs on a femtosecond time scale,[9−11] which could not be resolved in the studies of Moser et al. With the broad spectral range covered in our transient absorption measurements and the good spectral separation of the various species formed as a result of the charge injection from fluorescein 27 (D^{2-} for short), we can monitor the formation and decay of all the major species. The transient absorption spectrum of the fluorescein 27 molecule following femtosecond excitation reflects the dynamics of the ground and excited states and can therefore be used to monitor the electron injection and recombination. Since the injection quenches the excited state of the dye molecule, the fluorescence decay (or equivalently the stimulated emission decay) will be a sensitive marker of this process. The electron injection can also be monitored by the absorption spectrum of the electrons. Several groups have studied extensively the absorption spectra of excess electrons in the TiO_2 semiconductor.[17,19] Accordingly, it is known that these electrons have a broad and featureless absorption spectrum in the range 400−800 nm, with an absorption maximum around 620 nm and an absorption coefficient of 1200 1/(M* cm).[20] As shown previously by other authors, there is no absorption in this spectral region ($\lambda > 600$ nm) of the fluorescein dye or its oxidation products.[16,35] We also measured the transient absorption spectrum of fluorescein 27 in aqueous solution at pH ∼ 9 and no transients were observed in the spectral region of the injected electrons (data not shown). Therefore, it is possible to unambiguously detect the injected electrons. The detailed results of such measurements are presented in the next section.

The electron injection process could in principle also be monitored via the temporal evolution of the excited-state absorption of the dye molecule (i.e., absorption of D^{2-*}) and the semioxidized radical ($D^{-\bullet}$), as was done in nanosecond experiments on eosin by Moser et al.[8,13] However, the absorptions of these two species are quite similar,[13,16,35] which makes it difficult to clearly resolve the initial injection step ($D^{2-*} \rightarrow D^{-\bullet} + e^-$) by monitoring these species. Once formed, the decay of the semioxidized anion ($D^{-\bullet}$) can be monitored with the help of its absorption in the 450 nm region.[16,35]

II. Experimental Section

Nanosized colloidal titanium dioxide (TiO_2) particles were prepared by controlled hydrolysis of titanium tetrachloride ($TiCl_4$) as proposed by Kormann et al.[14] A volume of 3.5 mL of distilled $TiCl_4$ pre-chilled to −20 °C was added slowly to 900 mL of vigorously stirred deionized water at 1 °C. After continuous stirring for 30 min at this temperature, the reaction mixture was dialyzed for 2−3 h at room temperature using 4−6 L of deionized water to change the pH from 1.7 to 2.3. Following rotary evaporation at 30 °C, a slightly yellowish crystal-like powder was obtained, which could be resuspended in pure water, methanol, or ethanol (or mixtures of ethanol, methanol, and water) to obtain perfectly transparent colloidal TiO_2 suspensions. Transmission electron microscopy (TEM) was used to determine the average particle diameter of 2.4 nm of the semiconductor particles. Their crystal structure had previously been determined to be that of anatase.[14] The quality of the particles obtained in this work was tested measuring and analyzing the UV−vis spectrum of dissolved colloids following a method suggested by Kormann et al.[14] Thus, a plot of $\ln(\alpha)$ (α = absorption coefficient) as a function of the photon energy ($h\nu$) yields the band gap energy (E_{gap}) of 3.35 eV, identical to that obtained in ref 14 for 2.4 nm particles. The shift from $E_{gap} = 3.2$ eV for bulk anatase to $E_{gap} = 3.35$ eV for particles 2.4 nm in diameter is interpreted as a result of a quantum size effect. Therefore, we conclude that our preparation procedure, identical to that in ref 14, resulted in crystalline anatase particles with an average particle diameter of ≈2.4 nm. The distribution in particle size may be taken from a work of Serpone et al.[18] A mean particle diameter of 2.1 nm with a variance of 1.1 nm was reported for TiO_2 particles obtained with a comparable preparation method.

The fluorescein 27 laser dye was used as purchased from Lambda Physik. A fluorescein 27 saturated aqueous stock solution at pH 10 was prepared prior to each measurement and was used to obtain the desired concentration by adding a few microliters of this solution to a certain amount of water (usually 5−10 mL) at the desired pH. The final pH of the solution was determined using a Metrohm pH electrode which was calibrated using standard buffer solutions (Merck) prior to each measurement. For the experiments with colloidal TiO_2 solutions, a stock suspension of 100 g/L was prepared by dissolving the desired amount of TiO_2 powder.

Femtosecond transient absorption measurements were performed using a regeneratively mode-locked and amplified Ti: sapphire laser system pumping an optical parametric oscillator/amplifier (OPA) system. The OPA generated the excitation pulses at 530 nm, while the probe pulses were taken from a white light continuum generated by a part of the amplified fundamental laser beam at 800 nm, which was focused into a sapphire plate. For the data acquisition a monochromator and three photodiodes in a single-shot detection system was used. Details of this spectrometer can be found elsewhere.[42] The repetition rate of the excitation pulses was set to 5 kHz, and the energy was adjusted to 2 μJ/pulse. The light pulses were focused into a rotating sample cell with a 2 mm path length to a spot size of 200 μm, resulting in a photon density of 5×10^{14} photons/cm^2. Since the spectrum of the free dye in a pH 3 aqueous solution (shown as the dotted spectrum in Figure 4) has a more blue-shifted spectrum and a smaller absorbance than the adsorbed dye, we have chosen an excitation wavelength of 530 nm for our laser experiments to ensure a selective excitation of the adsorbed dye (Figure 4).

The transient absorption kinetics were fitted to the equation:

$$\text{Fit} = \int_0^t T(t-t')\, F(t')\, \mathrm{d}t' \tag{4}$$

The function $T(t - t')$ is the Gaussian pulse shape which was determined for each particular experiment from the transient absorption signal of the dye nile blue or fluorescein 27. The response function had a fwhm of ~150 fs. At most wavelengths the kinetic analysis resulted in a single-exponential rise time and a second-order decay plus a constant. The formula used for the fit is

$$F(t) = \frac{A_1(1 - A_2 \exp(-k_1 t))}{(1 + k_2 t)} + A_3 \tag{5}$$

In cases where no rise time was observed, we used the fit function:

$$F(t) = \frac{A_1}{(1 + k_2 t)} + A_3 \tag{6}$$

where A_i is the amplitude, k_i is a rate constant, k_1 is the first-order rate constant, and k_2 is the second-order rate constant.

For a multiexponential fit, the following function was used:

$$F(t) = \sum_i A_i * \exp(-k_i t) \tag{7}$$

The employed fitting procedure used pseudo-inverses for a best least-squares fit of the linear parameters (the amplitudes A_i) and a simplex routine for the best least-squares fit of the exponential rate constants. The fits were performed using Matlab software.[15]

III. Results

Before time-resolved experiments could be performed, the TiO_2/dye system had to be characterized with steady-state spectroscopy. Since TiO_2 particles previously have been investigated extensively, we focus our characterization of the system on the properties of the dye and its adsorption at the TiO_2 surface. As the pH of the solution is important for processes at semiconductor−water interfaces, the absorption spectrum of the dye in aqueous solution as a function of pH was studied first. It is well-known that a change of the acid−base equilibrium of the OH and COOH groups of the dye (see Figure 1) leads to a change of the π-electron distribution and therefore to a change in the absorption spectrum.[16] This change of the absorption spectrum as a function of pH was measured and analyzed employing a nonlinear fitting procedure to obtain the pK_a values for the protonation/deprotonation of the OH and COOH groups and thus the spectra of the differently charged dye species. Figure 2 presents the different spectra of the dianion, anion, neutral, and cationic dye species. The pK_a values for the protonation/deprotonation of the OH groups are determined to be pK_{a1} = 0.5 and pK_{a3} = 4.5, whereas we obtained pK_{a2} = 4.1 for the protonation/deprotonation of the COOH group. A more detailed discussion of the different dye species has been provided by Linquist et al. for a very similar fluorescein dye.[16]

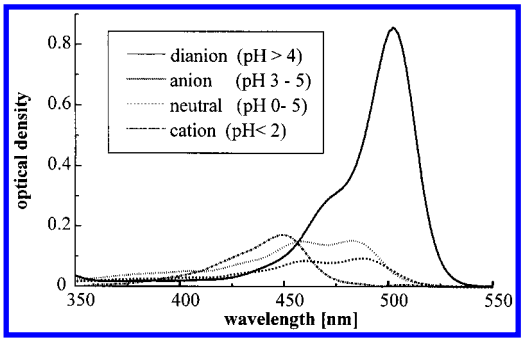

Figure 2. Absorption spectra of differently charged fluorescein 27 species: 13 μM fluorescein in aqueous solution, 1 cm optical path length. Spectra were obtained by a nonlinear least-squares fitting procedure. The pK_a values for the different species obtained from the fit are, 0.5 (neutral), 4 (anionic), and 4.5 (dianionic).

Figure 2 shows that the dianionic form of the dye, present at pH > 4, has an absorption maximum at 502 nm and a five times stronger absorbance than the other dye species in more acidic aqueous solution. The anionic form of the dye, present at pH 3−5, has two absorption maxima at 460 and 480 nm, very similar to the neutral form present from pH 0 to pH 5. Further protonation of the keto/enol group at pH < 1 leads to the cation form with a single absorption maximum at 450 nm. This spectral information is important for finding the optimum pH conditions for the adsorption of the dye at the TiO_2 surface in a colloidal TiO_2 suspension. Since the isoelectric point for the colloid is pH 5,[14] the particles are positively charged at pH < 5 and negatively charged at pH > 5. Optimum conditions for the chemisorption can be expected for strong electrostatic attraction between dye and surface, implying that one must find conditions where the TiO_2 surface is positively charged and the dye is negatively charged, while agglomeration of the particles is still prevented. This was accomplished by choosing pH 3 as the optimum pH.

Figure 3a,b shows the effect of increasing TiO_2 concentration on the absorption and fluorescence spectra of a solution of 4.2 μM fluorescein 27 at pH 3. The absorption spectrum without TiO_2 is mainly from the neutral form of the dye with some contribution from the monoanion. With increasing TiO_2 concentration the overall absorption increases and the maximum absorption shifts toward 490 nm. Simultaneous with the change of the absorption, the intensity of the fluorescence decreases to reach a constant value at high TiO_2 concentrations. Similar absorption and fluorescence changes have been found for other dyes in the presence of TiO_2 particles and were explained with the increasing amount of chemisorbed dye at the semiconductor surface. For a review of these investigations see ref 17 and references therein.

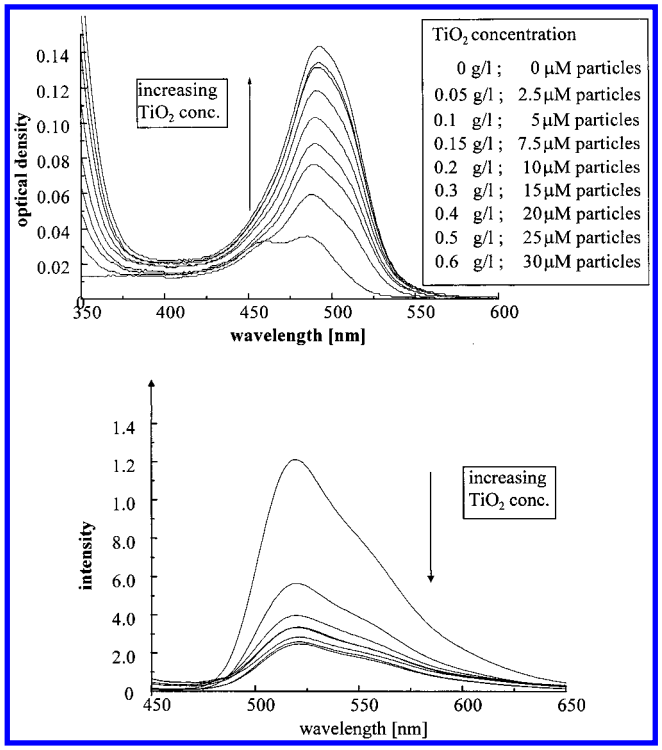

Figure 3. (a) Absorption spectra of fluorescein 27 in the presence of various TiO_2 concentrations. Conditions: 4.15 μM fluorescein 27 solution at pH 3, 1 cm optical path length. (b) Fluorescence intensity of fluorescein 27 in the presence of various TiO_2 concentrations. Conditions: 4.15 μM fluorescein 27 at pH 3, 1 cm optical path length, 440 nm excitation wavelength.

It is notable that the absorption spectrum in the presence of 30 μM TiO_2 is similar to the spectrum of the dianionic form of the dye in solution (see Figure 2), although the vibrational shoulder at 440 nm is absent and a shoulder at 510 nm is present if TiO_2 is added. This implies that the π-electron distribution of the adsorbed dye is similar to the non-adsorbed dianionic form. However, an assignment of the coordination of the dye at the TiO_2 surface would for instance require an infrared spectroscopy investigation which is beyond the scope of this paper.

On the basis of FTIR investigations performed by Hug et al.[39] with carboxylic acids we suggest the following adsorption mechanism (eq 8):

$$R - COO^- + \equiv Ti - OH_2^+ \overset{K}{\rightleftharpoons} \equiv Ti - OOC - R + H_2O \quad (8)$$

where K is an association constant.

The negatively charged fluorescein 27 dye ($R-COO^-$) reacts with a positively charged Ti−hydroxyl group and becomes bound to the surface Ti atom via a bidentate surface complex. We consider in eq 8 only the adsorption of the carboxylic group on the TiO_2 surface. However, an additional weaker interaction of the keto/enol group of the dye with the TiO_2 surface may lead to a tripod geometry with the dye in a flat orientation onto the surface.

With the assumption that the optical density at 530 nm is directly proportional to the concentration of adsorbed dye ($\equiv Ti-OOC-R$), the variation of optical density at 530 nm with TiO_2 particle concentration was analyzed by employing a simple Langmuir adsorption isotherm (eq 9). Since the particle concentration is proportional to the concentration of surface hydroxyl groups ($\equiv Ti-OH_2^+$), we can define an apparent association constant $K_A = C_{\equiv Ti-OOC-R}/(C_{TiO_2} \times C_{R-COO-})$ with

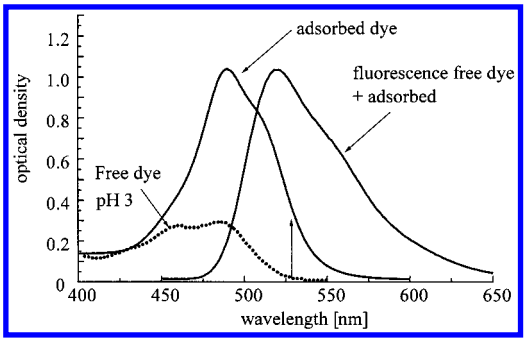

Figure 4. Absorption and fluorescence spectra of fluorescein 27. Dotted line: Absorption spectrum of 78 μM fluorescein 27 in aqueous pH 3 solution. Solid lines: 78 μM fluorescein in aqueous pH 3 solution with 85 μM colloidal TiO_2 particles, 2 mm optical path length. Fluorescence spectrum obtained by exciting at 440 nm. The arrow indicates the wavelength of laser excitation in the time-resolved experiments.

C_{TiO_2} = particle concentration, C_{R-COO-} = nonadsorbed dye concentration, and $C_{\equiv Ti-OOC-R}$ = surface complex concentration. With $C_{R-COO-} = C^0_{R-COO-} - C_{\equiv Ti-OOC-R}$ one obtains a Langmuir adsorption isotherm (eq 9)

$$C_{\equiv Ti-OOC-R} = C^0_{R-COO-} \times (K_A \times C_{TiO_2})(1 + K_A \times C_{TiO_2})^{-1} \quad (9)$$

where C^0_{R-COO-} = overall concentration of dye molecules.

A fit to the experimental adsorption data using eq 9 resulted in an excellent agreement, with an apparent association constant of $K_A = 7.6 \times 10^4\ M^{-1}$ (data not shown) for the data in Figure 3a. Therefore, we conclude that, preferentially, only one type of surface complex is formed since we would otherwise expect a deviation of the experimental data from eq 9 (see ref 39 for comparison). The value of the association constant is of the same order of magnitude as found with other sensitizing dyes, although a quantitative comparison is difficult since the particle size and modification as well as the solvent are different in other studied systems.[17]

For our time-resolved measurements we used a solution of 80 μM fluorescein 27 in the presence of 85 μM TiO_2 particles at pH 3. The absorption and fluorescence spectra of this solution are shown in Figure 4. The dotted spectrum in this figure indicates the absorption spectrum of fluorescein 27 at pH 3 in the absence of TiO_2.

With the association constant obtained from the Langmuir analysis we can now estimate the amount of dye adsorbed at the TiO_2 surface (eq 9). Under the experimental conditions of Figure 4 approximately 85% of the dye molecules are adsorbed, implying that on the average somewhat more than every second particle carries an adsorbed dye molecule. This enables us to study the electron injection reaction under well-defined conditions of an ensemble of particles each carrying one adsorbed dye molecule. Furthermore, we have excited only 2−5% of the adsorbed dye molecules, so any energy transfer between different dye molecules can be excluded. This was in addition confirmed by performing excitation-intensity-dependent kinetic measurements at 490 and 515 nm, which show a linear intensity dependence of the signal amplitude and intensity independent kinetics.

The very low probability of triplet state formation in the fluorescein 27 laser dye, combined with the nanosecond lifetime of its excited singlet state, strongly favors electron injection from the excited singlet state of the dye molecule into the TiO_2 semiconductor. This is revealed in the following by the analysis of our detailed kinetic data. We have monitored the electron

injection from the excited singlet state of the dye molecule into the TiO_2 semiconductor in several different ways, to unravel the different processes associated with the electron transfer. The decay of the excited state of the dye molecule linked to the injection process is monitored via the temporal evolution of the transient absorption spectrum following femtosecond pulse excitation of the dye. The transient absorption (ΔA) spectrum of the excited dye molecule carries information about dynamics of both the ground and excited states; bleaching of the ground state and stimulated emission from the excited state results in negative signal amplitudes, while absorption from the excited state (or any product state generated by the pulse excitation) yields a positive signal if these species absorb more strongly than the initial ground-state molecules. This implies that we can use the decay of the stimulated emission or excited-state absorption of the dye to monitor the excited-state quenching accompanying charge injection. In principle it should also be possible to use the appearance of the oxidized dye ($D^{-\bullet}$) to monitor the injection process. However, it turns out that for fluorescein 27 used here, the absorptions of the initially excited singlet state ($D^{2-}*$) and the oxidized dye ($D^{-\bullet}$) are quite similar (see below for details) and it is therefore quite difficult to use these species for monitoring of the charge injection. In addition we can use the characteristic absorption of the injected electrons, in the red and near-infrared part of the spectrum, to observe the appearance (and disappearance) of the electrons in the semiconductor. Finally, the decay of the electron population that occurs via recombination with the oxidized dye molecule ($D^{-\bullet}$) (see eq 3) can be visualized with the help of the recovery of the ground-state bleaching of the dye.

Figure 5a,b displays the transient absorption spectrum of fluorescein 27 in the wavelength region 410−580 nm, measured at increasingly later times after 530 nm excitation of a fluorescein 27/TiO_2 solution with the concentrations as shown in Figure 4. A negative differential absorption is found in the 470−580 nm range (Figure 5a) due to the ground-state bleaching and stimulated emission, whereas a positive signal, due to excited-state absorption and oxidized-dye absorption, is obtained from 410 to 470 nm (Figure 5b). The evolution of the spectral shape is complete within ∼500 fs, and at later delay times the overall signal decays almost uniformly to reach constant signal amplitudes at long times (τ > 50 ps, compare kinetics in Figure 5c).

The spectral change within the first ∼500 fs after excitation consists of a marked decay in the wavelength interval between 520 and 580 nm. At all other wavelengths the amplitude changes of the spectrum between 100 and 500 fs time delay are very small. After these initial spectral changes the shape of the spectrum remains almost constant and the average amplitude of the spectrum decreases to 30% of the initial value at 30 ps and to approximately 15% at times >50 ps. Furthermore, a closer inspection of the ΔA-spectrum in the 450−490 nm interval shows that the maximum of the spectrum shifts progressively from 425 to 460 nm with increasing time delay. This shift is complete at a time delay of ∼25 ps and suggests the presence of a relaxation process within the oxidized dye molecule. We will discuss this process below.

Direct measurement of kinetics provides more precise information of the temporal evolution of the spectral changes. Kinetics measured at several wavelengths (420, 470, 515, and 530 nm) throughout the transient absorption spectrum of fluorescein 27/TiO_2 are shown in Figure 5c. The trace measured at 530 nm depicts the decay of the stimulated emission and recovery of ground-state bleaching. An exponential fit requires

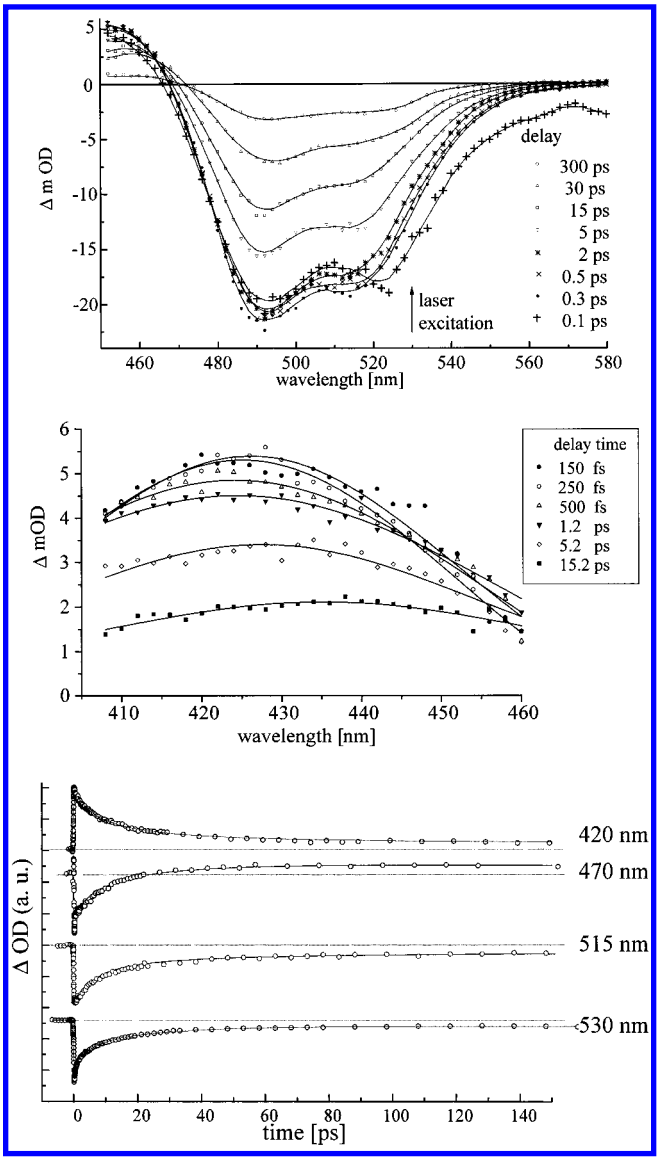

Figure 5. (a) Transient absorption spectra of adsorbed fluorescein 27 at different time delays. Concentrations and optical path length as indicated in caption of Figure 4. (b) Transient absorption spectra in the wavelength region 410−460 nm, at delay times from 150 fs to 15.2 ps as indicated. Concentrations and optical path length as indicated in caption of Figure 4. (c) Transient absorption kinetics at different wavelengths. Circles, measured points; solid lines, kinetic fits. Fit parameters are summarized in Table 1.

TABLE 1: Fit Parameters to Kinetics Measured in the Wavelength Range 420−900 nm

wavelength	first-order rate	second-order rate	const.
420 nm	350 fs (44.4% decay)	9.3 ps (51.2% decay)	4.4%
470 nm		12.8 ps (76.5% decay)	23.5%
515 nm	865 fs (18.4% rise)	10.1 ps (73% decay)	8.6%
530 nm	350 fs (22% decay)		10%
	4.9 ps (33.7% decay)		
	23 ps (34.3% decay)		
550 nm	300 fs (54% decay)		14%
	5.4 ps (32% decay)		
650 nm	500 fs (100% rise)	9.6 ps (60% decay)	40%
900 nm	300 fs (100% rise)	10 ps (73% decay)	27%

three time constants (350 fs, 4.9 ps, and 23 ps) and a constant background to reproduce the measured kinetics (the amplitudes of the various components are summarized in Table 1). The shortest decay time represents the decay of the stimulated emission (SE) and thus the electron injection, while the slower

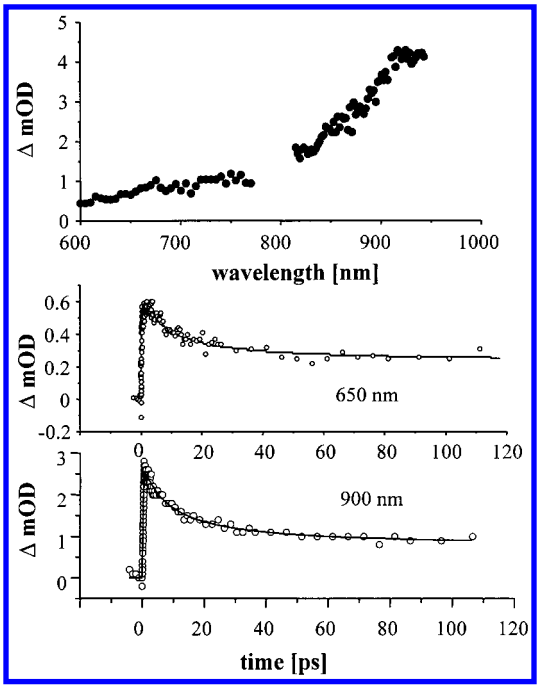

Figure 6. Uppermost panel: Transient absorption spectrum of fluorescein 27/TiO_2 in the wavelength region 600−950 nm, 1 ps after laser excitation at 530 nm. Experimental conditions as indicated in the legend of Figure 4. Two lower panels: Transient absorption kinetics at 650 and 900 nm; circles are measured data, lines are fits to eq 5. Fitting parameters are summarized in Table 1.

time constants correspond to the nonexponential recovery of the ground-state bleaching. For the shorter wavelengths of Figure 5c (420, 470, and 515 nm) the best fit is a second-order decay with a time constant of approximately 10 ps, a small amplitude of a 350−850 fs component, and a constant background. The fast ∼500 fs component of the kinetics at these wavelengths can, by comparison with the Δ*A*-spectra of Figure 5a,b, be seen to reflect the decay of excited-state absorption of the initially excited fluorescein 27 molecule and formation of the semioxidized radical anion. At 420 nm this is seen as a decay, while at 515 nm it appears as a rise time. In the kinetic trace measured at 470 nm there is a sharp oscillatory feature at $t = 0$, due to impulsive stimulated Raman scattering from the walls of the sample cell, which should not be confused with a fast kinetic component. The precision of the numerical value of this component is relatively low due to the low amplitude, but it is sufficiently close to the decay time constant of stimulated emission to be safely assigned to the time evolution of the excited-state absorption associated to the excited-state quenching accompanying the electron injection and formation of the semioxidized anion. The kinetics at 470 nm is informative in another respect; it starts out at short times as a bleaching of the ground-state absorption and decays at later times, when the ground-state bleaching of the dye has recovered, into an absorption. This clearly indicates the formation of the semioxidized radical anion product state. The measurement of absorption anisotropy decay also provided information about the time of electron injection. Transient absorption anisotropy measured at 490 nm displayed a decay from 0.4 to 0.25 with a 300 fs time constant (data not shown). This decay can be associated with the decay of the initially excited state to the semioxidized radical.

We have also used the spectral region of the injected electron itself (see Introduction) to monitor the injection and recombination of the photogenerated electron. Figure 6 shows the absorption spectrum in the interval from 600 to 950 nm,

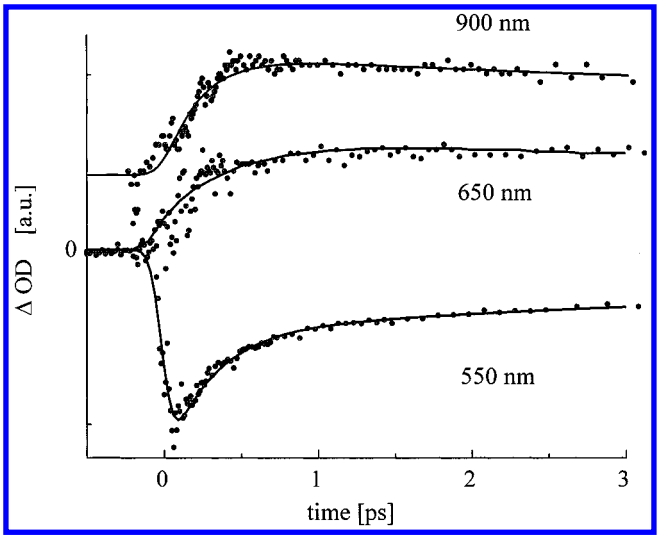

Figure 7. Comparison of fluorescein 27-stimulated emission decay and electron absorption rise times. Dots: Measured transient absorption kinetics at 650 and 900 nm are due to injected electrons, and the kinetics at 550 nm reflect the SE decay of fluorescein 27. Solid lines are fits, with the fitting parameters summarized in Table 1.

measured 1 ps after excitation. The absorption is very weak and featureless from 600 to 780 nm and rises steeply from 820 to 940 nm (the region from 780 to 820 nm could not be measured due to excessive scattered continuum pump-light). Examples of kinetics measured at 650 and 900 nm are also presented in Figure 6. The kinetic analysis (eq 5) of these data resulted in the same second-order half-lifetime of ∼10 ps as recovered in the 410−515 nm region. In Figure 7 the absorption transients are presented on a shorter time scale to visualize the rise time associated with formation of the electron absorption signal, 300 and 490 fs, respectively, that were obtained at 900 and 650 nm. Within the relatively large error of the 650 nm signal the rise times observed at 900 and 650 nm are considered to be equal. In addition, the rise of the 900 nm kinetics is superimposed by a weak oscillation, due to impulsive stimulated Raman scattering from the glass sample cell.[41] To further emphasize the identical decay of SE and rise time of the electron absorption, a SE decay measured at 550 nm is displayed in Figure 7 along with the kinetics of the electron absorption signal. Time constants and amplitudes are summarized in Table 1. In combination with the ∼300 fs SE decay, the ∼300 fs rise times of the electron signal unambiguously show that electrons are injected into the TiO_2 semiconductor from the photoexcited dye within this characteristic time.

IV. Discussion

1. Energetics of the Overall Process. In the following section, we discuss the energy scheme conventionally used for electron-transfer processes in photoelectrochemistry. All energies are given in eV scaled vs the standard redox potential of the normal hydrogen electrode (NHE). The absolute potential energy E_{abs} can be calculated from the standard redox potential E (V) obtained versus NHE with the relation[21]

$$E_{abs} = -4.5\ \text{eV} - eE \qquad (10)$$

where e = elementary charge.

The diagram in Figure 8 shows the electrochemical potentials of the valence band and the conduction band in the semiconductor and the electrochemical potential energy of the sensitizing dye molecule. We assume the potential of the conduction band

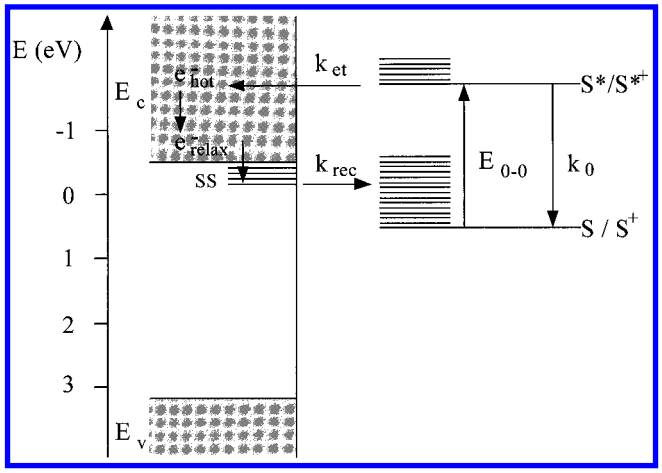

Figure 8. Mechanistic scheme for electron transfer from the electronically excited fluorescein 27 dye to TiO_2. The redox potential S/S^+ of the adsorbed dye is assumed to be the same as measured by cyclic voltammetry in aqueous solution at pH 8 in the absence of TiO_2. The E_{0-0} transition was obtained from the absorption and fluorescence steady-state spectra (Figure 4). S = dye; S*= excited dye; S^+ = oxidized dye; S^{*+} = electronically excited oxidized dye; E_c = conduction band; E_v = valence band; e^-_{hot} = hot electron; e^-_{relax} = relaxed electron; E_{0-0} = 0−0 transition of the dye (2.4 eV); k_0 = rate constant of radiative decay; S/S^+ = redox potential of the dye molecule ground state; S^*/S^{*+} = redox potential of the dye molecule excited state.

electrons in these nanosized particles to be approximately −0.3 eV at pH 3[22] and the electrochemical potential of the sensitizing dye to be 0.65 eV as measured by cyclic voltammetry[23] in homogeneous solution. This appears to be justified since cyclic voltammetric measurements by Heimer et al. of different sensitizing dyes in solution and when adsorbed at polycrystalline TiO_2 electrodes resulted in almost identical redox potentials.[44] The E_{0-0} transition of the adsorbed dye was taken from the absorption and fluorescence spectra to be 2.4 eV.

Under light excitation, fluorescein 27 is excited to a vibrationally hot state which thermalizes to the lowest vibrational state at a potential of −1.75 eV. This high redox potential of the excited molecule surely lies more than the reorganization energy above the edge of the conduction band potential, such that the electron injection into the semiconductor will therefore be an activationless process.[24,25] The reorganization energy of fluorescein 27 can be estimated from the Stokes shift of the fluorescence spectrum to be ≤0.3 eV. This appears to be a typical value for rigid molecules, since calculations by Moser et al.[7] of the solvent reorganization energy for coumarin-343, alizarin, and merocyanin Mc 2 adsorbed at TiO_2 nanoparticles in an ethanol−methanol mixture resulted in similar reorganization energies.

The electronically excited dye injects an electron into the semiconductor and a hot electron is created. This electron in the semiconductor thermalizes within some femtoseconds to the bottom of the wide conduction band.[30] Subsequently, from the level at the bottom of the conduction band the electron can migrate through the semiconductor and be trapped in surface states or any other energetically favorable traps.[26,27,28] Finally, the electrons can recombine with the semioxidized dye radical leading to the regeneration of the ground state of the dye. The energy conservation within the electron-transfer process requires acceptor states of equal energy as the energy of the electron (donor states) in the semiconductor or vice versa. We accounted for this in Figure 8 by the assignment of higher potential energies than the average ground-state redox potential of the dye. Alternatively, electronic donor states in the semiconductor with the same energy as the ground-state potential of the oxidized dye radical (deep trap states) would in principle also serve as explanation. As mentioned above, we assume here the redox potential of the electron to be close or equal to the conduction band potential of bulk TiO_2. For details, see ref 5, 24, 25, 30, 43 and references therein.

2. Electron Injection. First, we will focus on the dynamics of the charge injection process. Figure 6 shows the spectrum of the injected electron. To the best of our knowledge, this is the first report of the absorption spectrum of an electron injected from an excited dye molecule on a time scale of 1 ps. The spectrum in Figure 6 is different from time-resolved spectra of electrons in TiO_2 obtained in the picosecond to nanosecond time domain, where a broad absorption from 400 to 800 nm with a maximum around 650 nm is always reported.[22,28−30] These spectra were associated with electrons localized in shallow traps, energetically approximately 0.1−0.4 eV more positive than conduction band electrons.[37] As opposed to these observations, the spectrum obtained here 1 ps after the 150 fs excitation pulse is rising monotonically from 600 nm toward 950 nm without a distinct maximum, as expected for electronic intraband transitions or free electron absorption.[11,37,38] However, this time-resolved spectrum is in qualitative agreement with reported stationary spectra of polycrystalline TiO_2 films, interpreted as a mixture of intraband transitions and free carrier absorption.[37] It is noteworthy here that because of the small particles (d ∼ 2.4 nm), one electron is injected into a TiO_2 lattice consisting of approximately 250 TiO_2 molecules. This corresponds to a relatively high electron density of approximately 10^{20} cm^{-3} in the conduction band. Typical carrier densities used in semiconductor studies are in the range of $10^{15} - 10^{19}$ cm^{-3}.[30] Since intraband or free electron transitions should be proportional to the density of states in the conduction band, the particle size is decisive in determining the spectral properties under these conditions where exactly one dye molecule injects one electron into a semiconductor particle.

Very recent femtosecond experiments on TiO_2 with direct excitation of the semiconductor show a broad featureless absorption spectrum of the created electrons and holes similar to spectra obtained previously in the picosecond, nanosecond, and microsecond regime.[29] These spectra were measured from 400 to 760 nm at a delay of 500 fs and showed a maximum around 450 nm, the maximum of valence band hole absorption.[28,30] Because of the limited spectral region investigated in ref 29 and the overlapping of hole and electron spectra, a clear assignment of the pure electron spectrum appears to be difficult on the basis of these data. In conclusion, the spectrum in Figure 6 is interpreted as absorption of injected electrons. It is shown that the rise time of the electron absorption is ∼300 fs, which agrees well with the decay of the stimulated emission as shown in Figure 7. Therefore we conclude that the electron transfer occurs with a time constant of 300 fs.

In principle, an expression for the calculation of the rate constant of the electron injection may be obtained from the semiclassical Marcus equation for an activationless, nonadiabatic process.[31−33]

$$k_{ET} = \frac{2\pi}{h}|V|^2 (4\pi\lambda k_B T)^{-1/2} \qquad (11)$$

where $|V|$ = electronic matrix coupling element, λ = reorganization energy, k_B = Boltzmann constant, and h = Planck constant.

Taking a value of 0.01 eV for the electronic matrix coupling element and the assumed reorganization energy of 0.3 eV, an

injection rate of 300 fs is readily calculated. The value of 0.01 eV obtained for $|V|$ suggests the reaction to be on the borderline between the adiabatic and nonadiabatic mechanisms,[24,25] making the applicability of eq 11 somewhat uncertain. A quantum mechanical treatment of the electron injection process, taking into account the electronic structure of the dye and the semiconductor, could perhaps give a better explanation of the kinetics, but this is beyond the scope of this paper. For the sake of simplicity we evoke instead the classical Marcus equation. This equation enables us to discuss probable factors influencing the electron-transfer rate of the injection process in a qualitative way.

From eq 11, the classical Marcus expression can be retained for $\kappa \leq 1$ as

$$k_{ET} = \kappa\nu \tag{12}$$

where κ = transmission coefficient ($\kappa < 1$ for nonadiabatic reactions), and ν = frequency of nuclear motion through the transition state.

According to eq 12 the electron-transfer reaction can be considered to be adiabatic if the transmission coefficient κ equals 1. In that case, the electron injection is independent of $|V|$ and depends only on the frequency of nuclear motion through the transition-state region. With a typical frequency of $\nu > 100$ cm^{-1} for the slow motion of the nuclear coordinates, the experimentally observed reaction time of 300 fs suggests that the electron transfer follows the adiabatic mechanism.[24,25] The strong electronic coupling necessary for adiabaticity may be achieved by complexation of a surface Ti atom with the carboxylic acid group of the dye,[39] which thus mediates the electron transfer from the dye directly to the empty d-orbital manifold of the conduction band. In this context, recent reports of fast electron injection processes into TiO_2 also constitute evidence for a very strong electronic coupling.[9,11,12] The charge injection from excited perylene dyes was found to be temperature independent from 4 to 300 K, whereas temperature dependence is predicted from eq 11. Moreover, times as short as 80 fs and even 25 fs were reported[11,12] for charge injection into polycrystalline TiO_2 electrodes from chemisorbed perylene and ruthenium bipyridyl dyes under ultrahigh vacuum. With these very short injection times it appears that electron transfer may precede vibrational energy redistribution (violating the requirement of a vibrationally relaxed reactant in eq 11) and thus proceed from a vibrationally hot molecule.

3. The Recombination Reaction. As shown above, the transient absorption signal in the wavelength regions from 420 to 515 nm and 600−900 nm decays, after the first 500 fs, with the same kinetics. The best fit of this decay is a second-order kinetic equation plus a constant term (see eq 6), which produced a significantly better fit than a four-exponential fit function (eq 7). In addition, the plot of the reciprocal signal amplitude as a function of the delay time gives a linear dependence over the first 15 ps of the decay curves, as predicted from a second-order kinetic equation. Only in the wavelength region of the stimulated emission from 515 to 580 nm were different kinetics found. This difference is most likely due to the additional fast decaying amplitude of the stimulated emission and the small contribution of the ground-state bleaching of the dye in this spectral region.

The obtained second-order half-life time is ∼10 ps. This decay time is interpreted as the recombination of the electron with the dye, since the signal of the electron decays with exactly the same kinetics as the signal of the dye. At first sight the recombination between an electron and a semioxidized radical is a bimolecular process and should therefore obey a second-order rate law. However, under our experimental conditions only one electron and one semioxidized radical are present at each particle. Therefore, we deal with a geminate recombination where the injected electron always returns to the same dye molecule. For a similar case, the recombination of electron/hole pairs created in colloidal TiO_2 particles, Rothenberger et al.[20] have applied a stochastic model which resulted in a first-order kinetic law for less than 0.5 electron/hole-pairs per particle. However, recombination processes after electron injection of an excited dye into an semiconductor were studied by Moser et al,[7,8] and more recently by Fessenden et al.,[4] Yan et al.,[10] Tachibana et al.,[9] Ford et al.,[32] Hannappel et al.,[11] and Martini et al.[40] with a variety of different dyes. While results from Moser et al.[7,8] show a single-exponential recombination kinetics on the nanosecond and microsecond time scale, results from others usually show nonexponential recombination dynamics in the picosecond to microsecond time domain. The single-exponential recombination rates found with dye-sensitized colloidal TiO_2 particles by Moser et al.[7,8] were attributed to the recombination of the trapped electron and the radical associated as a radical pair state. It appears unlikely that this situation prevails during the first ∼300 ps (our time window) after injection of the electron into the semiconductor. However, the slowly decaying part of our kinetics (>100 ps) (Figures 5c and 6), which we did not examine in detail (and included as a constant background in our kinetic analysis), may correspond to the previously observed nanosecond and microsecond recombination processes as observed by Moser et al.[7,8]

In relation to the multiexponential recombination dynamics observed by others, the second-order kinetics, found to be the best fit to our experimental data, is merely phenomenological expressing the strongly nonexponential nature of the recombination process. Therefore, we cannot make conclusions from only the kinetics about details of the underlying mechanism of this recombination reaction. The kinetic nature of the recombination needs further mechanistic investigation, which must include variation of the particle size as well as the dispersion of particle size, and furthermore must consider all possibilities of trap states and the nature of the adsorbed dye.[11] However, for a qualitative treatment we invoke again the classical Marcus equation. This equation enables us to discuss probable factors influencing the electron-transfer rate of the recombination process.

$$k_{ET} = \kappa\nu \exp\left(-\frac{(\lambda + \Delta G^0)^2}{4\lambda k_B T}\right) \tag{13}$$

where $\Delta G^0 = (E_c - E_{S/S+})$, E_c = potential of electrons in the conduction band of the semiconductor, $E_{S/S+}$ =redox potential of adsorbed dye, λ = reorganization energy, and ν = nuclear frequency.

The electronic coupling for the recombination reaction should be the same as for the electron injection since the dye molecule is supposed to remain in the same geometrical orientation on this fast time scale. Therefore, the back reaction is also considered to be adiabatic (or at least on the borderline of the adiabatic mechanism) and thus $\kappa \sim 1$. In contrast to the electron injection, recombination requires activation energy. According to Figure 8 the back reaction is highly exergonic ($\Delta G^0 = -0.95$ eV), and therefore lies energetically in the inverted Marcus region. The activation energy in this approach is determined by the difference between the potential of electrons and the ground-state redox potential of the adsorbed dye molecule. For illustration, with a typical nuclear frequency of ∼100 cm^{-1}, a

reorganization energy of 0.3 eV, and $\Delta G^0 = -0.95$ eV (as obtained from Figure 8), one calculates a recombination rate constant of $(400\ \text{ns})^{-1}$. This value is a factor of 10^5 slower than the observed major (~85% amplitude, Figures 5a and 6) recombination rate of $\sim(10\ \text{ps})^{-1}$.

At this point, it is very interesting that we observe a shift of the absorption maximum in the spectrum shown in Figure 5b. As was explained in the Results section, the absorption spectrum in the wavelength region 410−470 nm at times >1 ps (Figure 5b) is associated with the nonrelaxed semioxidized radical anion. The ~25 ps red-shift of the anion ΔA-spectrum is therefore indicative of vibrational relaxation and cooling or perhaps structural relaxation of the hot radical anion, and a lowering of the potential energy of the radical, leading to an increase of ΔG^0 with time after the injection. Strictly, a spectral red shift implies that the S_0-S_1 energy gap is decreasing and we cannot be certain as to the extent of relaxation of the ground state. However, relaxation processes such as cooling, vibrational relaxation, solvation, or structural relaxation of the adsorbed dye molecule most likely shift both ground and excited states to lower energies. According to eq 13 this should result in a progressive decrease of the recombination rate with time. For example, for a reaction in which $\Delta G^0 = -0.65$ eV at $t = 0$, i.e., less exergonic by 0.3 eV, we obtain a recombination rate constant of 20 ps. Since the relaxation of the initially prepared hot semioxidized radical involves inner and outer vibrational processes, which occur on different time scales, we should expect a highly nonexponential recombination reaction. In that case, our fitting procedure with a second-order rate equation plus a constant accounts empirically for the highly nonexponential kinetics.

In conclusion of this section, the much slower back reaction as compared to the electron injection suggests that the recombination is in the Marcus inverted region where the recombination rate is slowed because of a highly exergonic reaction. Furthermore, the results suggest that the very wide distribution of recombination rates, ranging from ~25 picoseconds to nanoseconds, and perhaps microseconds is a result of a time-dependent ΔG^0 induced by vibrational relaxation, cooling, and perhaps solvation and structural relaxation of the anion product state.

As already mentioned above, multiexponential kinetics of recombination processes were also found in recent publications similar to that described here. In principle, a distribution of energetically different trap sites for electrons could be responsible for such highly nonexponetial kinetics. This was indeed suggested by Martini et al.[40] who explained the observed multiexponential recombination rate by the assignment of qualitatively different electronic trap states at the TiO_2 surface. Qualitatively, it is expected that different trap sites should have different optical transitions. However, no evidence for this could be found in our experiments, in which the recombination dynamics were recorded at different wavelengths in the electron absorption spectrum. At each investigated wavelength in the interval 600−950 nm (Figure 6), we found the same kinetics within experimental error. Therefore our experiments do not support the assignment of energetically different trap sites. Rather, our observation of a time-dependent spectral red shift of the radical anion spectrum provides strong evidence for a dynamic situation with a relaxation of ΔG^0 due to vibrational cooling and perhaps solvation and structural relaxation of the anion product state.

To obtain more information about the recombination reaction it would be interesting to perform experiments under conditions where more than one dye molecule is adsorbed per particle and thus several electrons could be injected. Under such conditions the apparent recombination time should be dramatically accelerated according to a second-order rate law. Furthermore, investigations of the temperature dependence of the injection and recombination rate would also be of great interest to provide additional data for the comparison with theoretical models. A preliminary account of this work has been published elsewhere.[45]

Acknowledgment. This work was funded by grants from the Swedish Natural Science Research Council, the Knut and Alice Wallenberg Foundation, and the Crafoord Foundation. We thank Dr A. P. Yartsev for expertise, technical assistance, and helpful discussions, Dr. I. Uhlendorf from the Institute of Applied Photovoltaics, Gelsenkirchen, Germany, for determining the redox potential of the fluorescein 27 dye, and Dr. J. L. Herek for critical reading of the manuscript.

References and Notes

(1) Ronald, D. T.; Sosnowsky, G. *Chem. Rev.* **1997**, *97*, 83.
(2) Tributsch, H.; Calvin, M. *Photochem. Photobiol.* **1972**, *16*, 261.
(3) Memming, R. *Photochem. Photobiol.* **1972**, *16*, 325.
(4) Fessenden, R. W.; Kamat, P. V. *J. Phys. Chem.* **1995**, *99*, 12902.
(5) Gerischer, H.; Willig, F. *Topic. Curr. Chem.* **1976**, *61*, 33.
(6) O'Regan, B.; Grätzel, M. *Nature* **1991**, *353*, 737.
(7) Moser, J. E.; Grätzel, M. *Chem. Phys.* **1993**, *176*, 493.
(8) Moser, J. E.; Grätzel, M. *J. Am. Chem. Soc.* **1984**, *106*, 6557.
(9) Tachibana, Y.; Moser, J. E.; Grätzel, M.; Klug, D. R.; Durrant, J. R. *J. Phys. Chem.* **1996**, *100*, 20056.
(10) Yan, S. G.; Hupp, J. T., *J. Phys. Chem.* **1996**, *100*, 6867−6870.
(11) Hannappel, T.; Burfeindt, B.; Storck, W.; Willig, F. *J. Phys. Chem.* **1997**, *101*, 6799.
(12) Burfeindt, B.; Hannappel, T.; Storck, W.; Willig, F. *J. Phys. Chem.* **1996**, *100*, 16436.
(13) Moser, J. E.; Grätzel, M.; Sharma, D. K.; Serpone, N. *Helvetica Chimica Acta* **1985**, *68*, 1686.
(14) Kormann, C.; Bahnemann, D. W.; Hoffmann, M. R. *J. Phys. Chem.* **1988**, *92*, 5196.
(15) *Matlab*; The Math Works, Inc., 24 Prime Park Way, Natick, MA 01760, 1992.
(16) Linquist, L. *Arkiv för Kemi* **1960**, *16*, 79.
(17) Kamat, K. V. *Chem. Rev.* **1993**, *93*, 267.
(18) Serpone, N.; Lawless, D.; Khairutdinov, R. *J. Phys. Chem.* **1995**, *99*, 16646.
(19) Hagfeldt, A.; Grätzel, M. *Chem. Rev.* **1995**, *95*, 49.
(20) Rothenberger, G.; Moser, J.; Grätzel, M.; Serpone, N.; Sharma, D. K. *J. Am. Chem. Soc.* **1985**, *107*, 8054.
(21) Lohmann, F. *Z. Naturforsch.* **1967**, *22a*, 843.
(22) Duonghong, D.; Ramsden, J.; Grätzel, M. *J. Am. Chem. Soc.* **1982**, *104*, 2977.
(23) Measurements performed by Dr. Ingo Uhlendorf, Institut for Applied Photovoltaics, Gelsenkirchen, 1997.
(24) Eichberger, R.; Willig, F. *Chem. Phys.* **1990**, *141*, 159.
(25) Willig, F.; Eichberger, R.; Sundaresan, N. S.; Parkinson, B. A. *J. Am. Chem. Soc.* **1990**, *112*, 2702.
(26) Skinner, D. E.; Colombo, D. P., Jr.; Cavaleri, J.; Bowman, R. M. *J. Phys. Chem.* **1995**, *99*, 7853.
(27) Colombo, D. P., Jr.; Bowman, R., M. *J. Phys. Chem.* **1996**, *100*, 18445.
(28) Bahnemann, D. W.; Hilgendorff, M.; Memming, R. *J. Phys. Chem. B* **1997**, *101*, 4265.
(29) Asahi, T.; Furube A.; Masuhara, H. *Chem. Phys. Lett.* **1997**, *275*, 234.
(30) Nozik, A.; Memming, R. *J. Phys. Chem.* **1996**, *100*, 13061.
(31) Sutin, N.; Brunschwig, B. S. *ACS Symp. Series* **1982**, *198*.
(32) Jortner, J. J. *Chem. Phys.* **1976**, *64*, 4860.
(33) Marcus, R. A.; Sutin, N. *Biochim. Biophys. Acta* **1985**, *811*, 265.
(34) Ford, W. E.; Wessels, J. M.; Rodgers, M. J. *J. Phys. Chem.* **1997**, *101*, 7435.
(35) Cordier, P.; Grossweiner, L. I. *J. Phys. Chem.* **1968**, *72*, 2018.
(36) Rehm, J. M.; Mclendon, G. L.; Nagasawa, Y.; Yoshihara, K.; Moser, J.; Grätzel, M. *J. Phys. Chem.* **1996**, *100*, 9577.
(37) Rothenberger, G.; Fitzmaurice, D.; Grätzel, M. *J. Phys. Chem.* **1992**, *96*, 5983.

(38) Sze, S. *Physics of Semiconductor Devices*, 2nd ed.; New York, 1981.
(39) Hug, S.; Sulzberger, B. *Langmuir* **1992**, *8*, 3587.
(40) Martini, I.; Hodack, J. H.; Hartland, G. V. *J. Phys. Chem. B* **1998**, *102*, 607.
(41) Hoy, Q.; Durrant, J. R.; Hastings, G.; Porter, G.; Klug, D. R. *Chem. Phys. Lett.* **1993**, *202*, 183.
(42) Chachisvilis, M. Electronic and Vibrational Coherence in Photosynthetic and Model Systems. Thesis, Department of Chemical Physics, Lund University, Sweden, 1996.
(43) Lewis, N. S. *Annu. Rev. Phys. Chem.* **1991**, *42*, 543.
(44) Heimer, T. A.; D'Arcangelis, S. T.; Farzad, F.; Stipkala, J. M.; Meyer, G. *Inorg. Chem.* **1996**, *35*, 5319.
(45) Hilgendorff, M.; Sundström, V. *Chem. Phys. Lett.* **1998**, *287*, 709.